Available online at www.sciencedirect.com
SCIENCE DIRECT®
Journal of Solid State Chemistry 173 (2003) 418–424
JOURNAL OF SOLID STATE CHEMISTRY
http://elsevier.com/locate/jssc

Tin–magnesium substitution in Ir_3Sn_7—structure and chemical bonding in $Mg_xIr_3Sn_{7-x}$ ($x = 0-1.67$)

Martin Schlüter,[a] Ulrich Häussermann,[b] Birgit Heying,[a] and Rainer Pöttgen[a,*]

[a] *Institut für Anorganische und Analytische Chemie, Universität Münster, Wilhelm-Klemm-Straße 8, 48149 Münster, Germany*
[b] *Department of Inorganic Chemistry, Stockholm University, 10691 Stockholm, Sweden*

Received 7 October 2002; accepted 25 February 2003

Abstract

Well-shaped single crystals of binary Ir_3Sn_7 were obtained from a tin flux (starting composition Ir:Sn = 1:10). The magnesium based stannides $Mg_xIr_3Sn_{7-x}$ ($x = 0.61-1.67$) were synthesized from the elements in glassy carbon crucibles in a water-cooled sample chamber of a high-frequency furnace. The samples were characterized by X-ray diffraction on powders and single crystals. All compounds crystallize with the cubic Ir_3Ge_7 type structure (space group $Im\bar{3}m$, $Z = 4$). In this structure type the *p*-block atoms occupy the Wyckoff positions 12*d* and 16*f* and form two interpenetrating frameworks consisting of cubes and square antiprisms. The transition metal atoms center the square antiprisms and are arranged in pairs. With increasing magnesium substitution the lattice parameter of Ir_3Sn_7 (935.3 pm) decreases from 934.7 pm ($x = 0.61$) to 930.6 pm ($x = 1.67$) and the Ir–Ir distances decrease from 294 pm (Ir_3Sn_7) to 290 pm ($Mg_{1.67}Ir_3Sn_{5.33}$). In the ternary compounds Mg substitutes Sn on both framework sites. However, the 12*d* site shows a substantially larger preference for Mg occupation. By performing first-principles calculations we investigated the bonding situation in Ir_3Sn_7 and its alteration upon Mg incorporation. For binary Ir_3Sn_7 there are considerable bonding interactions between Ir and Sn atoms (*d–p* bonding) and between neighboring Sn atoms on the site 16*f* (*p–p* bonding). Both types of interactions diminish when substituting Sn for Mg. This explains the different site preference of Mg in $Mg_xIr_3Sn_{7-x}$: Mg occupation of the site 12*d* retains covalent *p–p* framework bonding between 16*f* atoms in the ternary compounds.

Keywords: Intermetallic Compounds; Crystal structure; Chemical bonding; Tin

1. Introduction

In previous papers we reported on ternary intermetallic *RET*Mg compounds (*RE* = rare earth metal; *T* = transition metal), which are isotypic with *RET*In or *RET*Sn intermetallics ([1–3], and references therein). Surprisingly the magnesium atoms occupy positions that are typical for more electronegative elements. During phase analytical investigations of the ternary systems magnesium–transition metal–tin we obtained the new stannide $MgRuSn_4$ [4] which is isotypic with $LiRuSn_4$ [5–7]. Studies of the rhodium based system revealed a series of ternary stannides $Mg_xRh_3Sn_{7-x}$ ($x = 0.98-1.55$) with the Ir_3Ge_7 type structure [4,8]. This is a very remarkable result, in view of the non-existence of binary Rh_3Sn_7.

Representatives of the Ir_3Ge_7 structure type are typically compounds between 4*d* or 5*d* transition metals and a *p*-block element from the groups 13–16. We recently gave a detailed account of the bonding properties of these compounds and could identify two border situations of chemical bonding associated with Ir_3Ge_7 structure type [9]. Compounds from combinations of early transition metals with group 15 or 16 elements are characterized by strong *d–p* bonding. A *d–p* hybridization band gap is opened in the density of states and, depending on the electron count, narrow band gap semiconductors can be obtained. This is the case for $Nb_3Sb_2Te_5$ [10] and the recently described $Mo_3Sb_5Te_2$ [11]. In contrary, compounds from combinations of late transition metals with group 13 elements display a completely filled *d* band and strong *p–p* bonding within the *p*-block atom framework.

Here, we report on the synthesis and structural characterization of Ir_3Sn_7 and the solid solution $Mg_xIr_3Sn_{7-x}$ ($x = 0.61 - 1.67$). In contrast to Rh_3Sn_7,

*Corresponding author. Fax: +49-251-83-36002.
E-mail addresses: ulrich@inorg.su.se (U. Häussermann), pottgen@uni-muenster.de (R. Pöttgen).

0022-4596/03/$ - see front matter © 2003 Elsevier Inc. All rights reserved.
doi:10.1016/S0022-4596(03)00133-6

binary Ir_3Sn_7 is known but only approximate structural data were determined from early X-ray powder investigations [8]. According to our findings in Ref. [9], bonding in Ir_3Sn_7 should represent an intermediate situation between strong *d–p* (Ir–Sn) and strong *p–p* (Sn–Sn) bonding. We performed first-principles electronic structure calculations in order to explore the interesting electronic consequences when substituting a *p*-block metal (Sn) for an *s*-block one (Mg) in ternary $Mg_xIr_3Sn_{7-x}$.

2. Experimental

2.1. Synthesis

Starting materials for the synthesis of Ir_3Sn_7 and $Mg_xIr_3Sn_{7-x}$ ($x = 0.61 - 1.67$) were a magnesium rod (Johnson Matthey, ∅ 16 mm, >99.5%), iridium powder (Degussa-Hüls, 200 mesh, >99.9%), and tin as a bar (Heraeus, 99.9%) or in powder form (ABCR, >99.999%).

Binary Ir_3Sn_7 was prepared by mixing iridium and tin powder in a molar ratio of 1:10. The reactants were pressed into a pellet and loaded into a quartz ampoule, which was sealed under vacuum. The sample was heated to 873 K, annealed for 24 h and subsequently quenched in water. Excess tin was dissolved with 3 M HCl and the remains washed with deionized water. The reaction resulted in highly crystalline, phase pure, Ir_3Sn_7.

For synthesizing ternary $Mg_xIr_3Sn_{7-x}$ the magnesium rod and the tin bar were first cut into smaller pieces. The elements were subsequently weighed in the ideal atomic ratios, cold-pressed to pellets (∅ 6 mm) and put in small glassy carbon crucibles (SIGRADUR®G, glassy carbon, type GAZ006). The crucibles were placed in a water-cooled sample chamber made of DURAN® glass [12]. Homogeneous samples were obtained by high-frequency melting (Hüttinger Elektronik, Freiburg, Typ TIG 1.5/300) of the elements under flowing argon. The argon was purified over silica gel, molecular sieves, and titanium sponge (900 K). During the inductive heating process we first observe melting of tin which subsequently reacts with magnesium and iridium in an exothermic reaction. To ensure homogeneity and good crystallization the samples were held for 15 min at 800–900 K. No weight losses were observed. After cooling to room temperature, the samples could easily be separated from the glassy carbon crucibles by pounding at their base. No reaction of the samples with the crucibles could be detected. The samples are stable in air over several weeks. Single crystals exhibit metallic luster.

2.2. X-ray diffraction

The samples were characterized through Guinier powder diffractograms using Cu$K\alpha_1$ radiation and α-quartz ($a = 491.30$ pm, $c = 540.46$ pm) as an internal standard. The cubic lattice parameters (Table 1) were obtained from least-squares fits of the powder data. The correct indexing of the patterns was verified through

Table 1
Crystal data and structure refinement of Ir_3Sn_7, $Mg_{0.61}Ir_3Sn_{6.39}$, $Mg_{1.44}Ir_3Sn_{5.56}$, $Mg_{1.51}Ir_3Sn_{5.49}$ and $Mg_{1.67}Ir_3Sn_{5.33}$ (space group $Im\bar{3}m$; $Z = 4$)

Empirical formula	Ir_3Sn_7	$Mg_{0.61}Ir_3Sn_{6.39}$	$Mg_{1.44}Ir_3Sn_{5.56}$	$Mg_{1.51}Ir_3Sn_{5.49}$	$Mg_{1.67}Ir_3Sn_{5.33}$
Formula weight	1407.43	1349.62	1271.52	1264.95	1250.29
Unit cell dimensions	$a = 935.29(6)$ pm	$a = 934.74(6)$ pm	$a = 931.20(6)$ pm	$a = 931.17(6)$ pm	$a = 930.61(6)$ pm
(Single crystal data)	$V = 0.8182\,nm^3$	$V = 0.8167\,nm^3$	$V = 0.8075\,nm^3$	$V = 0.8074m^3$	$V = 0.8059\,nm^3$
Unit cell dimensions	$a = 936.7(1)$ pm	$a = 935.99(9)$ pm	$a = 934.5(1)$ pm	$a = 933.65(3)$ pm	$a = 933.8(1)$ pm
(Gunier powder data)	$V = 0.8217\,nm^3$	$V = 0.8200\,nm^3$	$V = 0.8160\,nm^3$	$V = 0.8139\,nm^3$	$V = 0.8142\,nm^3$
Calculated density	$11.43\,g/cm^3$	$10.98\,g/cm^3$	$10.46\,g/cm^3$	$10.41\,g/cm^3$	$10.30\,g/cm^3$
Crystal size	$20 \times 20 \times 30\,\mu m^3$	$30 \times 30 \times 60\,\mu m^3$	$30 \times 40 \times 60\,\mu m^3$	$40 \times 40 \times 50\,\mu m^3$	$30 \times 50 \times 50\,\mu m^3$
Transmission ratio (max/min)	1.21	2.36	1.27	2.58	1.58
Absorption coefficient	$69.5\,mm^{-1}$	$67.8\,mm^{-1}$	$66.1\,mm^{-1}$	$65.9\,mm^{-1}$	$65.6\,mm^{-1}$
$F(000)$	2324	2231	2105	2095	2071
θ range for data collection	3–35°	3–30°	3–35°	3–35°	3–40°
Range in hkl	± 13; ± 13; $-15 < l < 13$	± 13; ± 13; ± 13	± 14; ± 14; $-14 < l < 3$	$-13 < h < 14$; ± 14; $+14$	$+14$; ± 16; ± 16
Total no. of reflections	5218	4752	4518	3109	3815
Independent reflections	207 ($R_{int} = 0.0908$)	146 ($R_{int} = 0.0887$)	205 ($R_{int} = 0.1260$)	205 ($R_{int} = 0.1039$)	229 ($R_{int} = 0.1872$)
Reflections with $I > 2\sigma(I)$	180 ($R_{sigma} = 0.0278$)	129 ($R_{sigma} = 0.0198$)	182 ($R_{sigma} = 0.0371$)	155 ($R_{sigma} = 0.0329$)	158 ($R_{sigma} = 0.0534$)
Data/parameters	207/10	146/12	205/12	205/12	229/12
Goodness-of-fit on F^2	1.184	1.232	1.179	1.127	1.139
Final R indices[$I > 2\sigma(I)$]	$R_1 = 0.0221$	$R_1 = 0.0152$	$R_1 = 0.0259$	$R_1 = 0.0243$	$R_1 = 0.0391$
	$wR_2 = 0.0313$	$WR_2 = 0.0334$	$WR_2 = 0.0426$	$wR_2 = 0.0458$	$wR_2 = 0.0467$
R indices (all data)	$R_1 = 0.0370$	$R_1 = 0.0216$	$R_1 = 0.0313$	$R_1 = 0.0474$	$R_1 = 0.0741$
	$wR_2 = 0.0342$	$WR_2 = 0.0370$	$WR_2 = 0.0441$	$wR_2 = 0.0523$	$wR_2 = 0.0531$
Extinction coefficient	0.00274(9)	0.00096(6)	0.0104(4)	0.0014(1)	0.00138(8)
Largest diff. peak and hole	4.00 and $-2.46\,e/Å^3$	1.31 and $-1.47\,e/Å^3$	4.20 and $-1.97\,e/Å^3$	1.96 and $-2.13\,e/Å^3$	3.60 and $-2.69\,e/Å^3$

intensity calculations [13] taking the atomic positions from the structure refinements. The lattice parameters determined from the powders and the single crystals showed some discrepancies. This is most likely due to homogeneity ranges.

Single crystal intensity data were collected at room temperature by use of a four-circle diffractometer (CAD4) with graphite monochromatized Mo$K\alpha$ (71.073 pm) radiation and a scintillation counter with pulse height discrimination. The scans were taken in the $\omega/2\theta$ mode and empirical absorption corrections were applied on the basis of psi-scan data, followed by a spherical absorption correction. All relevant details concerning the data collections are listed in Table 1.

2.3. Structure refinements

Small, irregularly shaped single crystals of Ir_3Sn_7 and four magnesium substituted samples were examined by use of a Buerger camera equipped with an image plate system (Fujifilm BAS-1800) in order to establish suitability for intensity data collection. Analysis of the diffractometer data sets revealed body-centered cubic cells for all stannides and space group $Im\bar{3}m$ was found to be correct during the structure refinements in agreement with the previous investigation on the rhodium compounds [4].

The atomic parameters of $Mg_{0.98}Rh_3Sn_{6.02}$ [4] were taken as starting values and the structures were refined using SHELXL-97 [14] (full-matrix least-squares on F^2) with anisotropic atomic displacement parameters for all atoms.

As a check for the correct composition the occupancy parameters were refined in separate series of least-squares cycles along with the displacement parameters. All iridium sites and the tin sites of Ir_3Sn_7 were fully occupied within one standard deviation. These sites have been refined with the ideal occupancies in the final cycles. Similar to the $Mg_xRh_3Sn_{7-x}$ stannides, also the Sn1 and Sn2 sites of the iridium stannides showed mixed Sn/Mg occupancy. Subsequently tin-magnesium mixing was allowed on these positions and the occupancy parameters have been refined as a least-squares variable. The final difference Fourier synthesis were flat (Table 1). The highest residual peaks were all at the origin of the unit cell and most likely result from incomplete absorption corrections. The positional parameters and interatomic distances of the refinements are listed in Tables 2 and 3. Listings of the observed and calculated structure factors are available.[1]

[1] Details may be obtained from: Fachinformationszentrum Karlsruhe, D-76344 Eggenstein-Leopoldshafen (Germany), by quoting the Registry No's. CSD-412776 (Ir_3Sn_7), CSD-412777 ($Mg_{0.61}Ir_3Sn_{6.39}$), CSD-412778 ($Mg_{1.44}Ir_3Sn_{5.56}$), CSD-412779 ($Mg_{1.51}Ir_3Sn_{5.49}$), and CSD-412780 ($Mg_{1.67}Ir_3Sn_{5.33}$).

2.4. Electronic structure calculations

Total energy calculations for Ir_3Sn_7, $Mg_3Ir_3Sn_4$, $Mg_4Ir_3Sn_3$, and Mg_7Ir_3 were performed within ab initio density functional theory employing ultrasoft, Vanderbilt-like, pseudo-potentials and a plane wave basis set (program package VASP) [15–18]. Ir 5*d* and 6*s*, Sn 4*s* and 4*p*, and Mg 3*s* electrons were considered as valence electrons. All other electrons are described by the pseudo-potential. For all compositions atomic position parameters were relaxed for a set of constant volumes until forces had converged to less than 0.01 eV/Å. In a second step equilibrium volume V_{eq} and corresponding energy E_{eq} was obtained by fitting the obtained E vs V values to the Birch-Murnaghan equation of state [19]. The exchange and correlation energy was assessed by the local density approximation (LDA) [20]. Convergency of the calculations was checked with respect to the plane wave cut off and the number of k points used in the summation over the Brillouin zone. Concerning the plane wave cut off of an energy value of 300 eV was chosen. K points were generated by the Monkhost-Pack method [21] and sampled on $6\times6\times6$ grids. The integration over the Brillouin zone was performed with a Gaussian smearing of 20 mRy. Total energies were converged to better than 1 meV/atom.

3. Results and discussion

The structures of Ir_3Sn_7 and four magnesium substituted compounds $Mg_xIr_3Sn_{7-x}$ ($x = 0.61 - 1.67$) have been refined from X-ray single crystal diffractometer data. These stannides crystallize with the cubic Ir_3Ge_7 type structure (space group $Im\bar{3}m$). Ir atoms are located at the position 12*e* (x00) and the Mg/Sn atoms occupy the sites 16*f* (xxx) (Mg1/Sn1) and 12*e* (1/4 0 1/2) (Mg2/Sn2).

The iridium atoms in Ir_3Sn_7 and $Mg_xRh_3Sn_{7-x}$ have a square-antiprismatic tin/magnesium coordination. Two of these square antiprisms are condensed via a common square face forming the fundamental building unit of this structure (Fig. 1). These double prisms are aligned on each edge of the cubic unit cell. Thus, six double-prisms form a cube around each corner of the cell. The size of the cube is determined by the x parameter of the Mg1/Sn1 positions. As emphasized in Fig. 1, the complete structure consists of two interpenetrating frameworks which share the Sn2/Mg2 atoms.

An analysis of the geometrical features of the refined structures gave the following values: the x parameter of the iridium atoms first decreases from 0.34278 (Ir_3Sn_7) to 0.34247 ($x = 0.61$) and then increases to 0.3440 ($x = 1.67$). The x parameter of Sn1/Mg1, however, decreases continuously from 0.16500 to 0.1622 for the same substitution range. Thus, the Ir–Ir distances and

Table 2
Atomic parameters and equivalent isotropic displacement parameters (pm^2) of Ir_3Sn_7, $Mg_{0.61}Ir_3Sn_{6.39}$, $Mg_{1.44}Ir_3Sn_{5.56}$, $Mg_{1.51}Ir_3Sn_{5.49}$ and $Mg_{1.67}Ir_3Sn_{5.33}$ (space group $Im\bar{3}m$)

Atom	Wyckoff position	Occupancy[a]	x	y	z	U_{eq}
Ir_3Sn_7						
Ir	12*e*	1.00(4)	0.34278(5)	0	0	24(1)
Sn1	16*f*	1.00(4)	0.16500(5)	x	x	38(2)
Sn2	12*d*	1.00(4)	1/4	0	1/2	41(2)
$Mg_{0.61}Ir_3Sn_{6.39}$						
Ir	12*e*	1.00(1)	0.34247(5)	0	0	71(2)
Mg1/Sn1	16*f*	1.9(6)/98.1(6)	0.16404(5)	x	x	78(3)
Mg2/Sn2	12*d*	17.9(8)/82.1(8)	1/4	0	1/2	79(4)
$Mg_{1.44}Ir_3Sn_{5.56}$						
Ir	12*e*	1.00(1)	0.34367(5)	0	0	73(2)
Mg1/Sn1	16*f*	14.7(8)/85.3(8)	0.16266(5)	x	x	76(3)
Mg2/Sn2	12*d*	28.4(9)/71.6(9)	1/4	0	1/2	87(4)
$Mg_{1.51}Ir_3Sn_{5.49}$						
Ir	12*e*	1.00(1)	0.34397(8)	0	0	111(2)
Mg1/Sn1	16*f*	14.0(9)/86.0(9)	0.16230(8)	x	x	129(4)
Mg2/Sn2	12*d*	31.7(9)/68.3(9)	1/4	0	1/2	121(5)
$Mg_{1.67}Ir_3Sn_{5.33}$						
Ir	12*e*	1.00(1)	0.3440(1)	0	0	91(2)
Mg1/Sn1	16*f*	17(1)/83(1)	0.1622(1)	x	x	102(5)
Mg2/Sn2	12*d*	33(1)/67(1)	1/4	0	1/2	97(6)

[a] The occupancy parameters of the Ir and Sn positions of Ir_3Sn_7 and the Ir positions of $Mg_xIr_3Sn_{7-x}$ were obtained in separate series of least-squares cycles. In the final cycles the ideal occupancy values were assumed for these sites. The Mg1/Sn1 and Mg2/Sn2 occupancies were refined as least-squares variables for all $Mg_xIr_3Sn_{7-x}$ stannides.

Table 3
Interatomic distances in the stannides Ir_3Sn_7 and $Mg_xIr_3Sn_{7-x}$. All distances <400 pm are listed. They were calculated with the single crystal lattice parameters (standard deviations in parantheses). *M* denotes Sn in Ir_3Sn_7 and the Mg/Sn mixing in $Mg_xIr_3Sn_{7-x}$

		Ir_3Sn_7	$Mg_{0.61}Ir_3Sn_{6.39}$	$Mg_{1.44}Ir_3Sn_{5.56}$	$Mg_{1.51}Ir_3Sn_{5.49}$	$Mg_{1.67}Ir_3Sn_{5.33}$
Ir:	4 *M*1	274.4(1)	273.6(1)	272.6(1)	272.6(1)	272.4(1)
	4 *M*2	276.2(1)	276.2(1)	274.6(1)	274.4(1)	274.2(1)
	1 Ir	294.1(1)	294.5(1)	291.2(1)	290.6(1)	290.3(2)
*M*1:	3 Ir	274.4(1)	273.6(1)	272.6(1)	272.6(1)	272.4(1)
	1 *M*1	275.4(2)	278.4(1)	281.7(2)	282.9(3)	282.9(3)
	3 *M*1	308.7(1)	306.7(1)	302.9(1)	302.3(2)	302.0(2)
	6 *M*2	358.2(1)	358.6(1)	358.1(1)	358.3(1)	358.1(1)
*M*2:	4 Ir	276.2(1)	276.2(1)	274.6(1)	274.4(1)	274.2(1)
	4 *M*2	330.7(1)	330.5(1)	329.2(1)	329.2(1)	329.0(1)
	8 *M*1	358.2(1)	358.6(1)	358.1(1)	358.3(1)	358.1(1)

the size of the empty cubes slightly decrease. The smallest Ir–Ir distance of 290 pm in $Mg_{1.67}Rh_3Sn_{5.33}$, however, is somewhat longer than in fcc iridium (272 pm) [22].

Although the structural alterations upon tin substitution are rather small in $Mg_xIr_3Sn_{7-x}$ there are pronounced differences in the site occupancies of the positions 12*d* and 16*f*. There is a clear preference of magnesium to enter the framework site 12*d*. This is especially seen in $Mg_{0.61}Ir_3Sn_{6.39}$ with the lowest magnesium content. There the substitution almost exclusively affects the site 12*d*. With increasing magnesium content the site 16*f* also gets occupied by magnesium, however, the concentration of substituted tin is about twice as large on 12*d* (Table 2).

We performed total energy calculations for Ir_3Sn_7, $Mg_3Ir_3Sn_4$, $Mg_4Ir_3Sn_3$, and Mg_7Ir_3. The ternary compounds corresponded to ordered variants of the Ir_3Ge_7 structure, i.e., in $Mg_3Ir_3Sn_4$ magnesium and tin atoms occupy the sites 12*d* and 16*f*, respectively, and

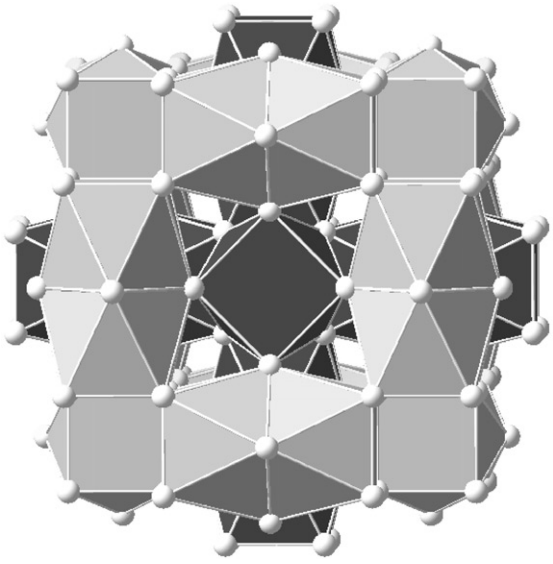

Fig. 1. The cubic crystal structures of Ir_3Sn_7 and $Mg_xIr_3Sn_{7-x}$. The two interpenetrating frameworks are shown. Details see text.

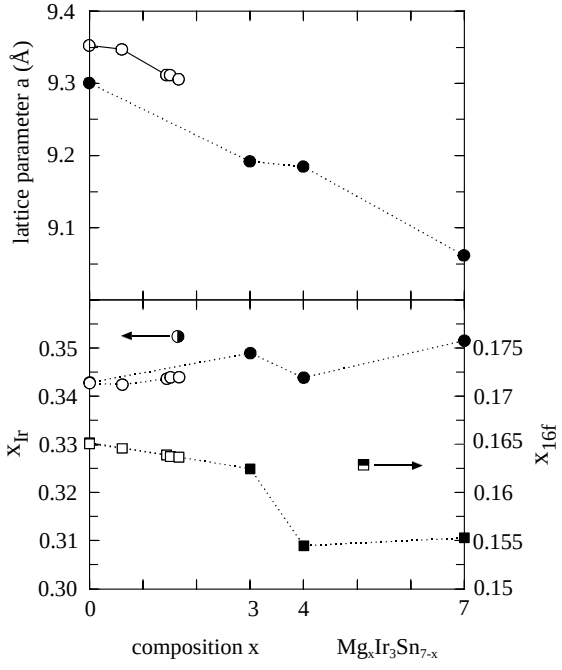

Fig. 2. Computed structural parameters for the compounds Ir_3Sn_7, $Mg_3Ir_3Sn_4$, $Mg_4Ir_3Sn_3$, and Mg_7Ir_3 (solid symbols). For comparison, the experimentally determined parameters of Ir_3Sn_7 and the solid solution $Mg_xIr_3Sn_{7-x}$ are also shown (open symbols).

vice versa in $Mg_4Ir_3Sn_3$. In Fig. 2 the calculated structural parameters are compiled and compared with the experimental ones. For binary Ir_3Sn_7 we observe excellent agreement between the theoretically and experimentally determined values. The computed lattice parameter is by about 0.6% lower than the experimental one, which corresponds to an underestimation of the ground-state volume by about 2%. The underestimation of ground-state volumes up to 5% (overbinding) is frequently observed when using LDA for assessing exchange and correlation energy. The experimental positional parameters of the site 16*f* in $Mg_xIr_3Sn_{7-x}$ are exactly on the connecting line of those for calculated Ir_3Sn_7 and $Mg_3Ir_3Sn_4$. The experimental *x* parameters of the iridium site 12*e* deviate somewhat from this line.

From $Mg_3Ir_3Sn_4$ to $Mg_4Ir_3Sn_3$ the computed structural parameters change discontinuously. A discontinuity is also observed in the trend of the bulk modulus and the energies of formation (Fig. 3). The bulk modulus B_0 is inverse to the compressibility of a material and parallels its hardness. B_0 decreases from 133 GPa in Ir_3Sn_7 to 80 GPa in hypothetical Mg_7Ir_3. This indicates a considerable weakening of the cubic materials overall bonding strength. The discontinuous trend from $Mg_3Ir_3Sn_4$ to $Mg_4Ir_3Sn_3$ shows that the destabilization is especially connected with the magnesium atoms being located on the 16*f* position. The trend in the energies of formation displays especially this destabilizing effect: the energy of formation decreases by about 35% when going from $Mg_3Ir_3Sn_4$ to $Mg_4Ir_3Sn_3$. As a matter of fact,

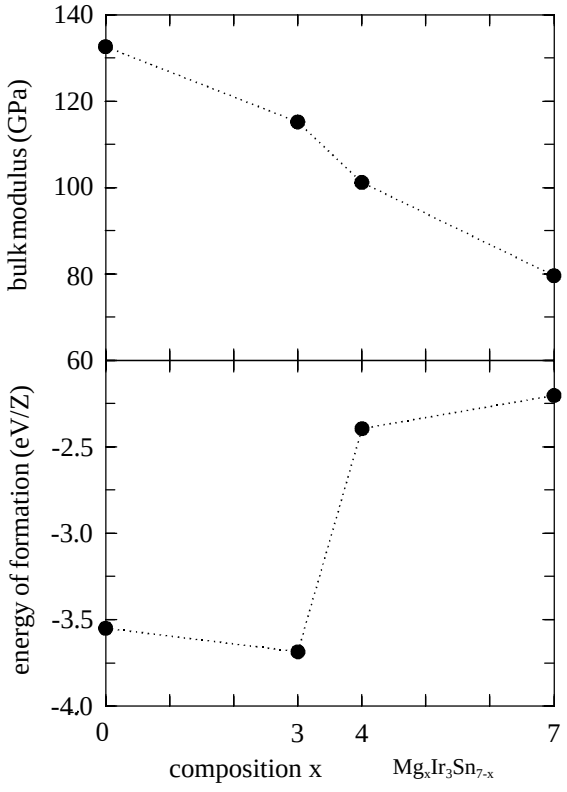

Fig. 3. Calculated bulk modulus and energy of formation (at zero Kelvin) for Ir_3Sn_7, $Mg_3Ir_3Sn_4$, $Mg_4Ir_3Sn_3$, and Mg_7Ir_3. The energies of formation are defined as $DE = E(Mg_xIr_3Sn_{7-x}) - xE(Mg) - 3E(Ir) - (7-x)E(Sn)$. The total energies of the elements are the equilibrium volume energy of the respective ground-state structures (hcp-Mg, fcc-Ir, α-Sn).

the latter compound would be unstable with respect to a mixture of $Mg_3Ir_3Sn_4$ and Mg_7Ir_3.

The trends in the calculated physical properties of $Mg_xIr_3Sn_{7-x}$ should also be reflected in the electronic structure. In Fig. 4 we compare the DOS of Ir_3Sn_7 with that of hypothetical Mg_7Ir_3 and in Fig. 5 valence charge distributions in these compounds are displayed. As expected for Ir_3Sn_7 the DOS reveal substantial *d–p* (Ir–Sn) bonding as is seen in the mixing of *d* and *p* based bands below and above the Fermi level. This interaction, however, is not strong enough to open a band gap in the DOS, instead a narrow, but deep, pseudo-gap is observed at the Fermi level. The considerable Ir–Sn bonding is also manifested in the valence charge distribution. We observe a pronounced accumulation of bond charge between iridium and Sn2 atoms in the (100) plane and between iridium and Sn1 atoms in the (110) plane. Additionally, the (110) plane reveals covalent *p–p* bonding interaction between neighboring Sn1 atoms located on site 16*f*. This site describes a bcc arrangement of (empty) cubes. The distance between two Sn1 atoms of neighboring cubes is only 275 pm in Ir_3Sn_7 and thus even shorter than the distance between singly bonded atoms in α-Sn (281 pm). The distance between two Sn2 atoms within the cubes (309 pm) compares to those in β-Sn (4×302 and 2×318 pm) [22].

The bonding situation in Mg_7Ir_3 is quite different to Ir_3Sn_7. Firstly, the dispersion of the *d*-based bands is smaller than in Ir_3Sn_7. This indicates that the Ir–Mg interactions are weaker than Ir–Sn ones. Interestingly, not only Mg-*s* but to a large extend also Mg-*p* states hybridize with Ir-*d* states. The Mg_7Ir_3 valence charge distribution is much more flat than in Ir_3Sn_7 and there is no pronounced bond charge accumulation between

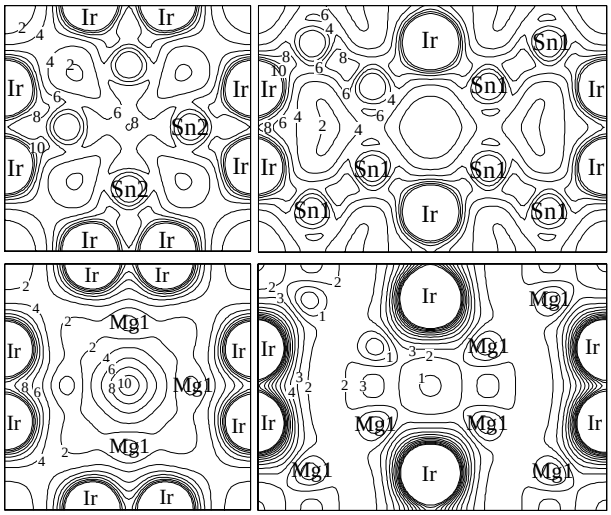

Fig. 5. Valence charge distributions in the (100) plane (left-hand side) and the (110) plane (right-hand side) of Ir_3Sn_7 (upper panel) and hypothetical Mg_7Ir_3 (lower panel). The charge distribution is presented in a range between 0.0 and 0.8 $e/Å^3$, contours are $n \times 0.04$ $e/Å^3$.

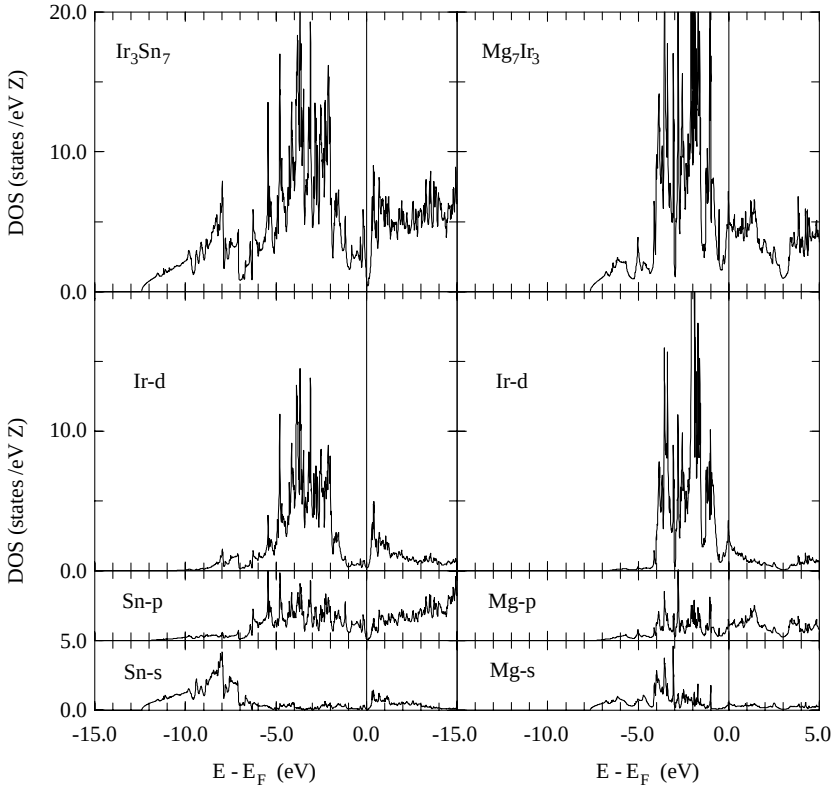

Fig. 4. Density of states of Ir_3Sn_7 and hypothetical Mg_7Ir_3 at the respective calculated equilibrium volumes.

iridium and magnesium atoms. Due to the smaller size of magnesium the unit cell volume of Mg_7Ir_3 is decreased compared to Ir_3Sn_7. As a consequence, the distance between the iridium atoms within the pairs becomes shorter and Ir–Ir bonding interactions develop. This is seen in an increase of valence charge between the iridium atoms within the pairs. However, most important is the loss of covalent bonding associated with the 16*f* site substructure, which becomes especially apparent when comparing the valence charge density distribution in the (110) planes of Ir_3Sn_7 and Mg_7Ir_3. We should note that the valence charge distribution in the planes (100) and (110) of $Mg_3Ir_3Sn_4$ virtually corresponds to that in the (100) plane of Mg_7Ir_3 and the (110) plane of Ir_3Sn_7, respectively, and vice versa for $Mg_4Ir_3Sn_3$. Thus, the loss of the covalently bonded Sn1 substructure is presumably the origin of the discontinuous trend in the physical properties when comparing the series of ordered compounds Ir_3Sn_7, $Mg_3Ir_3Sn_4$, $Mg_4Ir_3Sn_3$, and Mg_7Ir_3. The occupation of the site 16*f* by magnesium in $Mg_4Ir_3Sn_3$ leads to a destabilization, which agrees with the experimental observation that in the solid solution $Mg_xIr_3Sn_{7-x}$ magnesium preferentially segregates into the position 12*d* and that the maximum substitution concentration is rather small ($x \approx 1.67$).

In conclusion, our first-principles calculations show that the replacement of tin by magnesium in Ir_3Sn_7 leads to pronounced changes in the materials bonding properties. Mg (*sp*)–Ir (*d*) interactions are weaker than Sn (*p*)–Ir (*d*) ones. Additionally, the covalently bonded substructure of *p*-block Sn1 atoms in Ir_3Sn_7 cannot be retained with exclusively *s*–block magnesium atoms. In the structures of the compounds *RET*In and *RET*Sn [23] *p*-block atoms do not form a covalently bonded substructure and this might be the reason for the existence of the compounds *RET*Mg [3,24] with the *p*-block element being completely replaced by magnesium.

Acknowledgments

We are grateful to the Degussa-Hüls AG for a generous gift of iridium and to Dr. R.-D. Hoffmann and Dipl.-Ing. U.Ch. Rodewald for the intensity data collections. This work was financially supported by the Fonds der Chemischen Industrie, the Deutsche Forschungsgemeinschaft, and the Bundesministerium für Bildung, Wissenschaft, Forschung und Technologie.

References

[1] R. Mishra, R.-D. Hoffmann, R. Pöttgen, Z. Naturforsch. 56b (2001) 239.
[2] D. Johrendt, G. Kotzyba, H. Trill, B.D. Mosel, H. Eckert, Th. Fickenscher, R. Pöttgen, J. Solid State Chem. 164 (2002) 201.
[3] K. Łątka, R. Kmieć, A.W. Pacyna, T. Tomkowicz, R. Mishra, T. Fickenscher, H. Piotrowski, R.-D. Hoffmann, R. Pöttgen, J. Solid State Chem. 168 (2002) 331.
[4] M. Schlüter, A. Kunst, R. Pöttgen, Z. Anorg. Allg. Chem. 628 (2002) 2641.
[5] Zh. Wu, R.-D. Hoffmann, R. Pöttgen, Z. Anorg. Allg. Chem. 628 (2002) 1484.
[6] R. Pöttgen, Zh. Wu, R.-D. Hoffmann, G. Kotzyba, H. Trill, J. Senker, D. Johrendt, B.D. Mosel, H. Eckert, Heteroatom Chem. 13 (2002) 506.
[7] Zh. Wu, H. Eckert, J. Senker, D. Johrendt, G. Kotzyba, B.D. Mosel, H. Trill, R.-D. Hoffmann, R. Pöttgen, J. Phys. Chem. B 107 (2003) 1943.
[8] O. Nial, Svensk Kemisk Tidskrift 59 (1947) 165.
[9] U. Häussermann, M. Elding-Pontén, C. Svensson, Sven Lidin Chem. Eur. J. 4 (1998) 1007.
[10] P. Jensen, A. Kjekshus, J. Less-Common Met. 13 (1967) 357.
[11] E. Dashjav, A. Szczepenowska, H. Kleinke, J. Mater. Chem. 12 (2002) 345.
[12] D. Kußmann, R.-D. Hoffmann, R. Pöttgen, Z. Anorg. Allg. Chem. 624 (1998) 1727.
[13] K. Yvon, W. Jeitschko, E. Parthé, J. Appl. Crystallogr. 10 (1977) 73.
[14] G.M. Sheldrick, Shelxl-97, Program for Crystal Structure Refinement, University of Göttingen, 1997.
[15] G. Kresse, J. Hafner, Phys. Rev. B 47 (1993) 558.
[16] G. Kresse, J. Furthmüller, Phys. Rev. B 54 (1996) 11169.
[17] D. Vanderbilt, Phys. Rev. B 41 (1990) 7892.
[18] G. Kresse, J. Hafner, J. Phys.: Condens. Matter 6 (1994) 8245.
[19] J. Birch, J. Geophys. Rev. 57 (1952) 227.
[20] J.P. Perdew, A. Zunger, Phys. Rev. B 23 (1981) 5048.
[21] H.J. Monkhurst, J.D. Pack, Phys. Rev. B 13 (1976) 5188.
[22] J. Donohue, The Structures of the Elements, Wiley, New York, 1974.
[23] P. Villars, L.D. Calvert, Pearson's Handbook of Crystallographic Data for Intermetallic Compounds, 2nd Edition, American Society for Metals, Materials Park, OH, 1991 (Desk edition, 1997).
[24] B.J. Gibson, A. Das, R.K. Kremer, R.-D. Hoffmann, R. Pöttgen, J. Phys: Condens. Matter 14 (2002) 5173.